Correlating Nanoscale Structure with Ion Intercalation in Electrodeposited Nickel Hexacyanoferrate Thin Films

Kavita M. Jeerage,† William A. Steen,† and Daniel T. Schwartz*

Department of Chemical Engineering, University of Washington, Box 351750, Seattle, Washington 98195-1750

Received February 22, 2001. Revised Manuscript Received August 20, 2001

The relationship between the structure and ion intercalation in electrodeposited nickel hexacyanoferrate thin films is investigated using energy-dispersive X-ray (EDS) and Raman spectroscopies combined with electrochemical control of the iron centers' oxidation states. Nickel hexacyanoferrate thin films are prepared by cathodic deposition on a platinum substrate. Potential cycling in the range −100 to +900 mV vs saturated calomel electrode is used to reversibly intercalate and deintercalate K^+ from the matrix. Raman spectroscopy is used to determine the oxidation state of the iron centers, and EDS quantifies K^+ intercalation. Potential step changes are made between −100 and +900 mV, with spectroscopic analysis following each step change. A number of structural analogues to "soluble" and "insoluble" Prussian Blue are tested against the experimental results. The relationship between the amount of intercalated alkali cations and the oxidation state of the iron centers suggests that this material is nickel-rich, a result supported by X-ray photoelectron spectroscopy compositional analysis. These results are more consistent with a structure analogous to "insoluble", rather than "soluble", Prussian Blue, with the approximate unit cell stoichiometry $K_4Ni^{II}_4[Fe^{II}(CN)_6]_3$.

Introduction

Prussian Blue, an inorganic coordination compound with an open, zeolite-like structure, has been known for hundreds of years as a dye material. Prussian Blue contains a cubic framework of iron centers bound by cyanide bridges such that additional ions can intercalate into the interstitial sites. Prussian Blue was first prepared as a thin film on a conductive substrate in 1978.[1] Growth on a conductive substrate allows electrochemical control of the oxidation state of iron centers in the film via an applied potential. In the case of Prussian Blue, potential modulation causes dramatic color changes. As a result, this material has been extensively studied for its electrochromic properties.[2−5]

Prussian Blue is initially electrodeposited in the "insoluble" form,[6] with a unit cell formula of $Fe^{III}_4[Fe^{II}(CN)_6]_3$, which contains no interstitial ions. Upon potential cycling in K^+-containing solutions, the material undergoes a structural transformation to the "soluble" form,[4,7] with a unit cell formula of $K_4Fe^{III}_4[Fe^{II}(CN)_6]_4$. This material can be reduced to $K_8Fe^{II}_4[Fe^{II}(CN)_6]_4$ or oxidized to $Fe^{III}_4[Fe^{III}(CN)_6]_4$, with K^+ intercalation or deintercalation accompanying the oxidation state changes. In "soluble" Prussian Blue, all iron centers are octahedrally coordinated. "Insoluble" Prussian Blue differs by a single $Fe(CN)_6^{4-/3-}$ vacancy from the center of each cubic unit cell.

Other transition metal (cobalt, nickel, silver, cadmium, etc.) hexacyanoferrates, sometimes called Prussian Blue analogues, have also been prepared as thin films on conductive substrates; these analogues possess unique ion intercalation, electrochromic, and electrocatalytic properties.[8−10] In particular, modulating the valence of the iron centers in nickel hexacyanoferrate (NiHCF) thin films drives a reversible intercalation/deintercalation of charge-compensating alkali cations. This trait has been exploited for ion sensor[11,12] and ion-exchange[13−15] applications.

NiHCF thin films have been successfully grown by two basic methods: anodic derivatization of a nickel surface[16] and cathodic deposition onto a conductive

* To whom correspondence should be addressed.
† These authors contributed equally to this work.

(1) Neff, V. D. *J. Electrochem. Soc.* **1978**, *125*, 886.
(2) Ellis, D.; Eckhoff, M.; Neff, V. D. *J. Phys. Chem.* **1981**, *85*, 1225.
(3) Itaya, K.; Shibayama, K.; Akahoshi, H.; Toshima, S. *J. Appl. Phys.* **1982**, *53*, 804.
(4) Mortimer, R. J.; Rosseinsky, D. R. *J. Chem. Soc., Dalton Trans.* **1984**, 2059.
(5) Rajan, K. P.; Neff, V. D. *J. Phys. Chem.* **1982**, *86*, 4361.
(6) Itaya, K.; Ataka, T.; Toshima, S. *J. Am. Chem. Soc.* **1982**, *104*, 4767.
(7) Feldman, B. J.; Melroy, O. R. *J. Electroanal. Chem.* **1987**, *234*, 213.
(8) Bacskai, J.; Martinusz, K.; Czirok, E.; Inzelt, G.; Kulesza, P. J.; Malik, M. A. *J. Electroanal. Chem.* **1995**, *385*, 241.
(9) Dostal, A.; Hermes, M.; Scholz, F. *J. Electroanal. Chem.* **1996**, *415*, 133.
(10) Kulesza, P. J.; Malik, M. A.; Miecznikowski, K.; Wolkiewicz, A.; Zamponi, S.; Berrettoni, M.; Marassi, R. *J. Electrochem. Soc.* **1996**, *143*, L10.
(11) Amos, L. J.; Duggal, A.; Mirsky, E. J.; Ragonesi, P.; Bocarsly, A. B.; Bocarsly, P. A. F. *Anal. Chem.* **1988**, *60*, 245.
(12) Coon, D. R.; Amos, L. J.; Bocarsly, A. B.; Bocarsly, P. A. F. *Anal. Chem.* **1998**, *70*, 3137.
(13) Jeerage, K. M.; Schwartz, D. T. *Sep. Sci. Technol.* **2000**, *35*, 2375.
(14) Lilga, M. A.; Orth, R. J.; Sukamto, J. P. H.; Haight, S. M.; Schwartz, D. T. *Sep. Purif. Technol.* **1997**, *11*, 147.
(15) Rassat, S. D.; Sukamto, J. H.; Orth, R. J.; Lilga, M. A.; Hallen, R. T. *Sep. Purif. Technol.* **1999**, *15*, 207.
(16) Bocarsly, A. B.; Sinha, S. *J. Electroanal. Chem.* **1982**, *137*, 157.

10.1021/cm010156d CCC: $22.00
Published on Web 01/23/2002

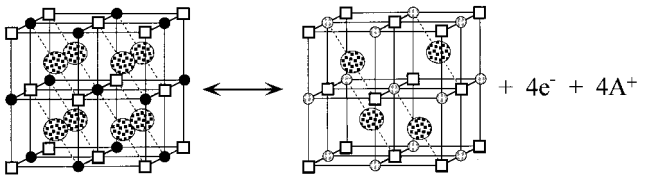

Figure 1. Unit cell representation of the redox reaction described by eq 1. In this figure, small black circles denote Fe(II), small gray circles denote Fe(III), open squares denote Ni(II), and solid lines denote the cyanide bridges. The large patterned circles denote intercalated alkali cations, whereas A^+ denotes the deintercalated cations in solution.

substrate.[8] In anodic derivatization, the film forms upon oxidation of nickel in the presence of ferricyanide anions. In cathodic deposition, the film forms via reduction of ferricyanide from marginally stable solutions containing divalent nickel, a process analogous to Prussian Blue deposition. Ion-exchange capacities for cathodically deposited films are normally much greater than those for anodically derivatized films, though many of their cation intercalation traits appear identical.[13,15]

The elemental composition of solution-precipitated NiHCF materials, which have been studied more than electrodeposited NiHCF materials, has been shown to vary greatly depending on the exact method of preparation. These materials are often described by the formula $A_{2z}Ni^{II}_{2-z}Fe^{II}(CN)_6$, where A represents any alkali cation and z varies from 0.1 to 1.2.[17] For example, the measured composition $Na_{0.98}Ni^{II}_{1.51}Fe^{II}(CN)_6$ corresponds to $z \approx 0.5$. However, compositions ranging from $K_{1.36}Ni^{II}_{1.07}Fe^{II}(CN)_6$ to $K_{0.03}Ni^{II}_{1.81}Fe^{II}(CN)_6$ (which must contain unmeasured protons or have partially oxidized iron centers to be charge balanced) have been reported for (nominally) identical precipitates.[18]

Despite the stoichiometric variation found in solution-precipitated NiHCF materials and the multiple structures of Prussian Blue that are known, electrodeposited NiHCF thin films are typically ascribed the stoichiometry $A_2Ni^{II}Fe^{II}(CN)_6$. This translates into the following electrochemically reversible redox reaction:

$$A_2Ni^{II}Fe^{II}(CN)_6 \leftrightarrow A_{2-x}Ni^{II}Fe^{II+x}(CN)_6 + xe^- + xA^+ \quad (1)$$

where x is the fraction of iron centers in the ferric oxidation state.[13−15,19−22] Figure 1 shows the unit cell representation of eq 1, which requires eight intercalated A^+ in the reduced state and four A^+ in the oxidized state. More generally, eq 1 implies that the oxidized state contains half as many charge-balancing alkali cations as the reduced state. The structure shown in Figure 1 is analogous to the Keggin−Miles structure for "soluble" Prussian Blue, with Ni(II) and interstitial A^+ replacing Fe(III).[23] The lattice constant for Figure 1 is ca. 10.2 Å.[17]

The first XRD results for anodically derivatized NiHCF materials have recently been reported by Kelly et al.[24] Despite the intrinsic difficulty of acquiring high-quality XRD data from the small quantities of derivatized material grown on electrodes, these studies showed unambiguously that the lattice constant varies systematically over the approximate range 10.17−10.22 Å, depending on the intercalated alkali cation and the oxidation state of the iron centers. These XRD results were combined with electrochemical data to propose the formation of secondary structures (microdomains) when mixtures of alkali cations of different sizes intercalate into the lattice. Because of the modest signal-to-noise ratios inherent in these experiments, only the (200), (220), (222), (400), and (420) reflections were observed. These reflections are common to both "soluble" and "insoluble" Prussian Blue lattices.[25] In short, although a great deal is now known about the secondary structure, questions remain about the primary structure of electrochemically prepared NiHCF.

Published results raise some doubts as to whether the structure shown in Figure 1 is indeed the true structure of electrodeposited NiHCF thin films. In a series of quartz crystal microbalance (QCM) measurements using H_2O and D_2O, Lasky and Buttry measured the incorporation of 3.2 H_2O for each Cs^+ expelled from the thin film upon Fe oxidation.[26] They noted that approximate molar volumes for Cs^+ and H_2O would suggest that only 0.67 H_2O should be incorporated for each Cs^+ expelled. Because postulating a water density within the matrix of nearly 5 times greater than the bulk value seemed unreasonable, they instead attributed their results to a large effective volume for Cs^+ which precludes H_2O incorporation into the 5 Å cubic intercalation site. However, using more accurate hard-sphere approximations, Schneemeyer et al. estimated the intercalation site to have a radius of 1.8 Å, just large enough to accommodate bare Cs^+, which has a 1.7 Å ionic radius.[22] In short, 3.2 H_2O could not fit into an intercalation site of the dimensions shown in Figure 1 without assuming anomalous behavior by the solvent.

We present experimental evidence which supports a more open, nickel-rich structure that deviates from the assumed "soluble" Prussian Blue analogue shown in Figure 1. Because XRD results that unambiguously determine the primary structure of electrochemically prepared NiHCF are difficult to acquire, we chose an alternate approach based on differences in the cation content of different structures. (N.B. For ion-exchange applications, our main interest, this characteristic is also of great importance.) Cation intercalation is investigated over a continuous range of oxidation states. Raman spectroscopy is used to determine the fraction of iron centers in the ferric oxidation state, and thin-film energy-dispersive X-ray spectroscopy (EDS) is used

(17) Loos-Neskovic, C.; Fedoroff, M.; Garnier, E.; Gravereau, P. *Talanta* **1984**, *31*, 1133.
(18) Loos-Neskovic, C.; Fedoroff, M.; Garnier, E. *Talanta* **1989**, *36*, 749.
(19) Humphrey, B. D.; Sinha, S.; Bocarsly, A. B. *J. Phys. Chem.* **1984**, *88*, 736.
(20) Humphrey, B. D.; Sinha, S.; Bocarsly, A. B. *J. Phys. Chem.* **1987**, *91*, 586.
(21) Kulesza, P. J.; Malik, M. A.; Skorek, J.; Miecznikowski, K.; Zamponi, S.; Berrettoni, M.; Giorgetti, M.; Marassi, R. *J. Electrochem. Soc.* **1999**, *146*, 3757.
(22) Schneemeyer, L. F.; Spengler, S. E.; Murphy, D. W. *Inorg. Chem.* **1985**, *24*, 3044.
(23) Keggins, J. F.; Miles, F. D. *Nature* **1936**, *137*, 577.
(24) Kelly, M. T.; Arbuckle-Keil, G. A.; Johnson, L. A.; Su, E. Y.; Amos, L. J.; Chun, J. K. M.; Bocarsly, A. B. *J. Electroanal. Chem.* **2001**, *500*, 311.
(25) Buser, H. J.; Schwarzenbach, D.; Petter, W.; Ludi, A. *Inorg. Chem.* **1977**, *16*, 2704.
(26) Lasky, S. J.; Buttry, D. A. *J. Am. Chem. Soc.* **1988**, *110*, 6258.

to evaluate the alkali cation content. The relationship between the ferric iron fraction and the amount of intercalated alkali cations is used to test a range of theoretical structures. These results point to a primary structure more closely related to the "insoluble", rather than the "soluble", analogue for electrodeposited NiHCF. The proposed structure is supported by compositional analysis using XPS.

Experimental Section

Electrochemistry. All studies employed a PAR 273A potentiostat controlled by custom LabVIEW software. A platinum disk electrode of 5 mm diameter and 1 mm thickness was mirror polished, mounted to an aluminum rod with conductive silver epoxy, and suspended such that the various electrolyte solutions wet a single (0.196 cm^2) face. All reported potentials are referenced to a saturated calomel electrode.

Energy-Dispersive X-ray Spectroscopy (EDS). A scanning electron microscope (JEOL JSM-5200) operated at an accelerating voltage of 15 or 20 keV was used to stimulate X-ray emission. Characteristic X-rays with energies between 0 and 10 keV were collected using a Si(Li) detector with a Be window (Link Systems). This permits identification of elements with $Z > 10$. Each spectrum was acquired for 10 min over a 1000 × 1000 μm region. After background subtraction via a locally weighted least-squares error method, the peaks were fit to a Gaussian function using a least-squares routine to calculate intensities.

Raman Spectroscopy. Spectra were generated using the 647.1 nm line of a Kr^+ laser (Coherent Innova 90) at 300 mW nominal laser power. Plasma emissions from the laser were removed using a band-pass filter (Omega Optical). The laser was focused using an f/10 spherical lens. Scattered light was collected at 90° from the incident beam by an f/1.2 Nikon camera lens, focused through a pinhole aperture, and collimated using an f/4 lens. The collimated light was passed through an OD6 holographic notch filter (Kaiser Optical) and refocused onto the 200 μm entrance slit of the spectrograph (Spex 270M) using another f/4 lens. An 1800 groove/mm grating dispersed the inelastically scattered light onto a liquid-nitrogen-cooled CCD detector (Princeton Instruments). Each spectrum was acquired for 30 s and filtered to remove cosmic spikes. The baseline was then removed, and the spectral wavenumbers were calibrated using the plasma emissions from the Kr^+ source.

XPS. An Al $K\alpha_{1,2}$ monochromatized X-ray source was used to stimulate photoemission from a 1000 × 1700 μm elliptical spot using a Surface Science Instruments (SSI) S-Probe. The energy of the emitted electrons was measured with a hemispherical energy analyzer at a pass energy of 150 eV. SSI data analysis software was used to calculate the elemental compositions from the corrected peak areas. Depth profile spectra were collected by masking the wide-angle acceptance lens with a 12° slit. The sample was rotated about an axis perpendicular to the analyzer lens axis and in the plane of the X-ray beam. Spectra were collected with the analyzer at 80°, 55°, and 0° with respect to the surface normal of the sample which probes approximately 20, 50, and 100 Å into the thin film, respectively.

NiHCF Deposition. The polycrystalline platinum substrate was electrochemically cleaned by repeatedly cycling the potential between −275 and +1675 mV at 100 mV/s in 1 M H_2SO_4. To deposit a film, the potential on the platinum substrate was cycled between +850 and 0 mV at 25 mV/s in freshly prepared 0.002 M $NiSO_4$, 0.002 M $K_3Fe(CN)_6$, and 0.25 M Na_2SO_4. It was then thoroughly rinsed with deionized water and dried. The reversible ion-exchange capacity was determined from the average of the integrated charge during the anodic and cathodic sweeps of the cyclic voltammogram. The NiHCF thin films used in this study had ion-exchange capacities between 10 and 18 mC/cm^2.

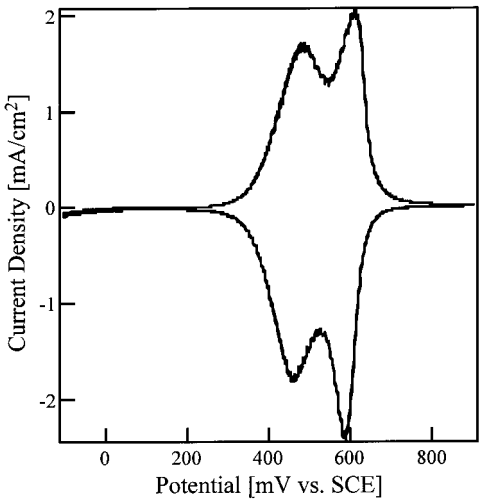

Figure 2. Voltammograms from a NiHCF thin film cycled 25 times in 1 M KNO_3 at 25 mV/s (every fifth cycle is shown).

Potassium Intercalation. Potential cycling in 1 M KNO_3 between −100 and +900 mV at 25 mV/s was used to exchange any Na^+ remaining from the deposition process. After 25 cycles, the potential was held at −100 mV for 5 min to reduce the NiHCF thin film and load it with K^+. The film was emersed from solution while still under potential control, then quickly rinsed, and dried in air. Raman and EDS spectra were acquired next (in that order). Then the film was reimmersed in a 1 M KNO_3 solution, and the potential was held at −100 mV for 1 min, followed by a step change to +300 mV, where the potential was held for 4 min. Again Raman and EDS spectra followed emersion, rinsing, and drying. This procedure was repeated in 100 mV increments until the film was fully oxidized at +900 mV.

Additional Samples. Three NiHCF thin films were examined by Raman and EDS in their fully reduced and fully oxidized states only. Two of these films were cycled 25 times in 1 M KNO_3 between −25 and +1125 mV at 25 mV/s; then one was held at −25 mV, and the other was held at +1125 mV, each for 15 min. The third film was cycled 25 times in 1 M $CsNO_3$ between the same limits and held at −25 mV for 15 min. All three NiHCF thin films were examined by Raman and EDS spectroscopy. Then the reduced films were ramped from −25 to +1125 mV at 25 mV/s, held there for 15 min, and reanalyzed with Raman and EDS. Similarly, the single-oxidized film was ramped from +1125 to −25 mV at 25 mV/s, held there for 15 min, and reanalyzed. Four additional NiHCF thin films were analyzed by XPS for elemental composition. These films were cycled 25 times in 1 M KNO_3 between −25 and +1125 mV at 25 mV/s. Then two films were held at −25 mV for 15 min, and the other two were held at +1125 mV, followed by XPS analysis.

Results and Discussion

General Characteristics of K Intercalation. Figure 2 shows the typical reversible electrochemical behavior of an electrodeposited NiHCF thin film cycled between −100 and +900 mV in a K^+-containing solution. Positive currents correspond to the oxidation of iron centers in the film, with the corresponding deintercalation of K^+ from the matrix, whereas negative currents correspond to iron reduction and K^+ intercalation. The double anodic and cathodic peaks in Figure 2 are unique to K^+-intercalated films. These peaks are perhaps due to multiple NiHCF phases within the thin film,[8] though the methods used here cannot readily test this. Nonetheless, we show later that the primary

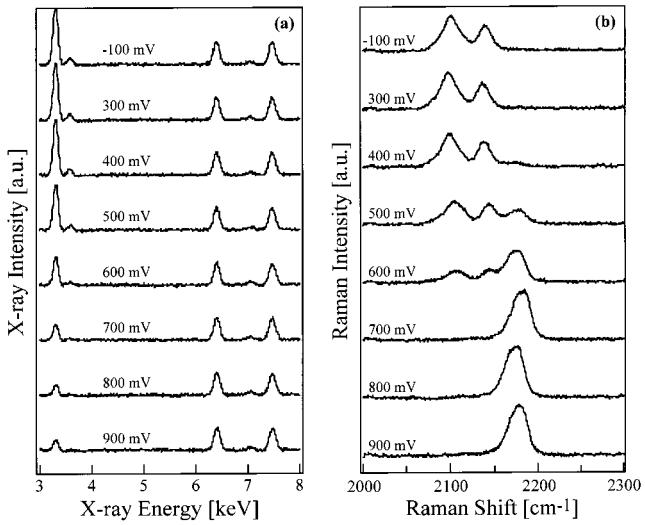

Figure 3. (a) Baseline-subtracted and normalized EDS spectra from a NiHCF thin film equilibrated at a series of potentials in 1 M KNO_3. The X-ray energy range does not include the large Pt peaks observed at ca. 2 and 9.4 keV. (b) Baseline-subtracted and normalized Raman spectra from a NiHCF thin film equilibrated at a series of potentials in 1 M KNO_3.

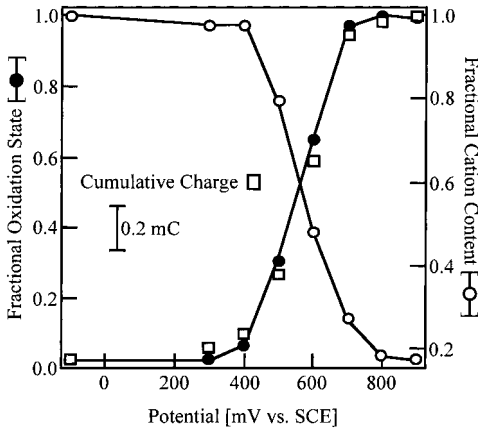

Figure 4. Ferric iron fraction, cumulative charge, and fractional cation content versus the potential at which the NiHCF thin film was equilibrated.

structure is not specific to K^+-intercalated films, despite their unique voltammetry.

Figure 3a shows ex-situ EDS spectra, after equilibration at each potential under consideration, from the same NiHCF thin film as in Figure 2. The K Kα (3.311 keV), Fe Kα (6.402 keV), and Ni Kα (7.204 keV) spectral peaks are large and well-defined. C and N (from cyanide) are not detectable. Because the incident electrons easily penetrate through the entire NiHCF film and into the Pt substrate, a thin film analysis is possible (see details of the analysis in work by Jeerage and Schwartz[13]). This means that when each spectrum is normalized by its Fe intensity, its K intensity is linearly proportional to the amount of K^+ in the NiHCF thin film. At −100 mV, the reduced film contains the maximum amount of intercalated K^+. As the potential is increased, the amount of K^+ decreases. The most dramatic change occurs between 400 and 700 mV, which corresponds to the potential window where current flows during cyclic voltammetry (Figure 2). Above 700 mV, the film is oxidized and the amount of K^+ has reached a minimum. We define the fractional cation content, *y*, relative to the maximum amount of intercalated K^+. That is, $y = I_K/I_{K,RED}$ where I_K is the Fe-normalized K X-ray intensity at any potential and $I_{K,RED}$ is the measured K intensity (also Fe-normalized) at −100 mV. Thus, *y* is set equal to 1 when the film is fully reduced and should equal 0.5, according to eq 1, when the film is fully oxidized. Comparing the spectra at +900 and −100 mV shows that this is not the case. Instead, *y* drops to less than 0.2. To determine whether these results are inconsistent with the assumed redox structure described by eq 1 and shown in Figure 1, we need to know the oxidation state of the iron centers; i.e., is the film fully reduced at −100 mV and fully oxidized at +900 mV. We can quantitatively determine the oxidation state of the iron centers with Raman spectroscopy.

Figure 3b shows ex-situ Raman spectra of the cyanide stretching region from the same NiHCF thin film as that in Figure 3a. The cyanide stretching modes are known to be sensitive to the oxidation state of the coordinating metals. At the potentials employed here, Ni maintains a formal charge of +2. Therefore, changes in the Raman spectra are due to oxidation state changes in Fe.[27] Cyanide coordinated to Fe(II) has two low-wavenumber peaks at 2102 and 2144 cm^{-1}, whereas cyanide coordinated to Fe(III) has a single resolvable high-wavenumber peak at 2186 cm^{-1}. At −100 mV, we expect the film to be fully reduced, and the presence of two low-wavenumber peaks confirms this. As the potential of the film is increased to 400 mV, a high-wavenumber peak begins to appear. By 700 mV, only the high-wavenumber peak is present, indicating that the film is fully oxidized. The region between 400 and 700 mV, where the film is changing rapidly from reduced to oxidized, again corresponds to the potential window where current flows during cyclic voltammetry (Figure 2). Principal component regression (PCR) of the Raman spectra allows calculation of the fraction of ferric iron, *x*, which is 0 when the film is fully reduced and 1 when the film is fully oxidized. The PCR model was built using calibration data acquired from both in-situ and ex-situ Raman measurements of NiHCF thin films cycled in Na^+-, K^+-, and Cs^+-containing solutions and is an extension of a previously published method.[27]

Figure 4 illustrates the correspondence between properties measured electrochemically and spectroscopically. The cumulative charge was calculated by integrating the current passed during each potential step change. The total charge passed was 1.71 mC. The fractional cation content, *y*, determined independently by ex-situ EDS spectroscopy, shows a close inverse relationship to the cumulative charge. The ferric iron fraction, *x*, determined independently by ex-situ Raman spectroscopy, follows the cumulative charge very closely. The excellent correspondence between these ex-situ spectroscopies and in-situ electrochemical measurements, as shown here and for many other samples, provides confidence in each respective measurement. More information can be gleaned by reducing the EDS and Raman results shown in Figure 4 to a single plot of fractional cation content (*y*) against the ferric iron

(27) Haight, S. M.; Schwartz, D. T.; Lilga, M. A. *J. Electrochem. Soc.* **1999**, *146*, 1866.

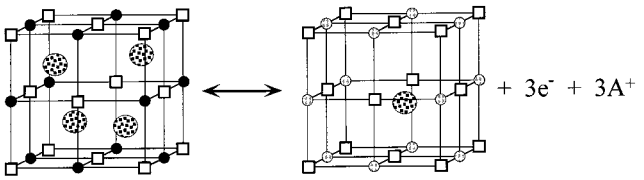

Figure 5. Unit cell representation of the redox reaction described by eq 2. In this figure, small black circles denote Fe(II), small gray circles denote Fe(III), open squares denote Ni(II), and solid lines denote the cyanide bridges. The large patterned circles denote intercalated alkali cations, whereas A^+ denotes the deintercalated cations in solution.

fraction (x). We call this a redox/structure plot because it will allow us to test structural models of the redox reaction in electrodeposited NiHCF thin films.

Comparison of Experimental Results with Theoretical Structures. In the redox reaction described by eq 1 and shown in Figure 1, four out of eight cations are expelled upon oxidation from Fe(II) to Fe(III). Thus, the fractional cation content (y) drops to 0.5 as the ferric iron fraction (x) goes from 0 to 1. On a redox/structure plot, this is represented by a line with the equation $y = -0.5x + 1$. As discussed previously, this structure is analogous to "soluble" Prussian Blue. However, if a structure analogous to "insoluble" Prussian Blue is considered instead, then one $Fe(CN)_6^{4-/3-}$ is removed from the center of each unit cell and the redox reaction in eq 1 is replaced by

$$A_{1.33}Ni^{II}{}_{1.33}Fe^{II}(CN)_6 \leftrightarrow A_{1.33-x}Ni^{II}{}_{1.33}Fe^{II+x}(CN)_6 + xe^- + xA^+ \quad (2)$$

which has the unit cell representation shown in Figure 5. In this structure, three out of four cations are expelled upon Fe oxidation, so the fractional cation content drops to 0.25 as the ferric iron fraction goes from 0 to 1. On a redox/structure plot, this reaction has the equation $y = -0.75x + 1$. More generally, we can define n as the number of $Fe(CN)_6^{4-/3-}$ vacancies per unit cell. On a redox/structure plot, all possible structures with this type of vacancy are represented by the equation

$$y = \left[\frac{4-3n}{8-4n} - 1\right]x + 1 \quad (3)$$

where n can vary from 0 (the assumed NiHCF structure) to $^4/_3$. When n is equal to $^4/_3$, the oxidized NiHCF matrix contains no cations and the redox reaction in eq 1 is replaced by

$$ANi^{II}{}_{1.5}Fe^{II}(CN)_6 \leftrightarrow A_{1-x}Ni^{II}{}_{1.5}Fe^{II+x}(CN)_6 + xe^- + xA^+ \quad (4)$$

The vacancy number, n, cannot go above $^4/_3$ because the oxidized matrix would then contain too much positive charge, requiring some other charge compensation process (anion intercalation, for example).

The combined EDS and Raman data can be fit to eq 3 to compare the overall stoichiometry of redox switching in electrodeposited NiHCF thin films with theoretical structures on the redox/structure plot. Figure 6 shows experimental data from Figure 3 as filled circles. Lines that represent the three structures just discussed

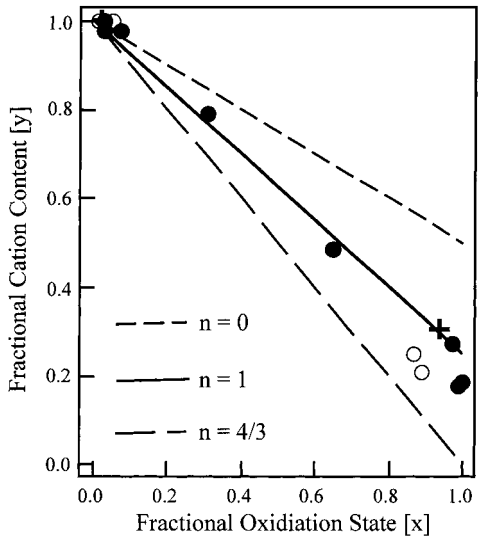

Figure 6. Redox/structure plot showing predicted behavior for a "soluble" Prussian Blue analogue ($n = 0$), an "insoluble" Prussian Blue analogue ($n = 1$), and a highly $Fe(CN)_6^{4-/3-}$ vacant structure ($n = {}^4/_3$). Experimental data for K^+-intercalated films (filled circles = main samples, open circles = additional samples) are consistent with either revised structure. Experimental data for a single Cs^+-intercalated film (crosses) are consistent with an "insoluble" Prussian Blue analogue.

are also included. Fitting the data to a linear equation by least-squares regression yields $y = -0.8x + 1$, which gives a vacancy number (n) equal to 1.09. This is quite close to the line expected for the redox structure described by eq 2 and shown in Figure 5. This structure has one vacant $Fe(CN)_6^{4-/3-}$ site per unit cell, leading to a more open, nickel-rich structure with 1.33 Ni for every Fe. Partially occupied $Fe(CN)_6^{4-/3-}$ sites have been previously observed (by XRD) in single crystals of $Ni_3[Fe^{II}(CN)_6]_2$ and $Ni_2Fe^{II}(CN)_6$.[18] Data from two additional K^+-intercalated films are indicated by open circles; these data also suggest a structure intermediate between the $n = 1$ and $^4/_3$ structures. Finally, data from one Cs^+-intercalated film is indicated by crosses. The Cs^+-intercalation data is most consistent with the $n = 1$ structure. The voltammetry of Cs^+-intercalated films is quite different from that of K^+ (one voltammetric peak vs two). The close agreement between Cs^+- and K^+-intercalated films on a redox/structure plot suggests that we are probing a primary structure that, on average, is not specific to K^+-intercalated films.

The compositional implications of these structural conclusions were tested by XPS compositional analysis. Angle-profiling studies which probed 20, 50, and 100 Å into the film found no composition variation with depth, although depths greater than 100 Å could not be analyzed. XPS analysis of four different NiHCF thin films (two oxidized and two reduced) confirms that the structures are nickel-rich, with two films having Ni:Fe ratios of 1.16 and the others being 1.17 and 1.23. Cataldi et al.[28] and Kulesza et al.[21] have reported Ni:Fe ratios equal to 1 (by XPS) and 1.08 (by AA), respectively. Disagreement may be due to subtlely different prepara-

(28) Cataldi, T. R. I.; Guascito, R.; Salvi, A. M. *J. Electroanal. Chem.* **1996**, *417*, 83.

tion procedures; we also note that the typical electrochemical response of our films differs from theirs.

The proposed nickel-rich structure suggested by the data in Figure 6 could result from interstitial Ni(II) replacing some cations (as opposed to the open "insoluble" Prussian Blue analogue proposed). The QCM experiments of Lasky and Buttry indirectly address this issue.[26] As noted earlier, fitting the experimentally measured amount of water into the interstitial space of a "soluble" Prussian Blue analogue is unlikely. The presence of interstitial Ni(II) would only exacerbate this problem. Furthermore, the literature for solution-precipitated NiHCF materials with nickel-rich compositions tend to have unit cells with iron vacancies rather than interstitial Ni(II).[29] These facts suggest that interstitial Ni(II) is not the cause of the observed nickel-rich structure.

The experimental data shown in Figure 6 could also result from a material composed of two distinct phases. A material composed of $^1/_4$ "soluble" Prussian Blue analogue (eq 1, $n = 0$) and $^3/_4$ highly $Fe(CN)_6^{4-/3-}$ vacant structure (eq 4, $n = {}^4/_3$) would have the same average composition as an "insoluble" Prussian Blue analogue (eq 2, $n = 1$). Multiple electroactive forms of NiHCF have been postulated by Bacskai et al.[8] as well as Kelly et al.[24] to explain double oxidation and reduction peaks. Bacskai et al. hypothesized that eq 4 corresponds to the low potential redox peaks and eq 1 corresponds to the high potential peaks, while Kelly et al. postulated the formation of microdomains with different intercalated cation compositions. Unfortunately, our method cannot resolve whether multiple forms exist. Because one alkali cation deintercalates for each electron withdrawn from the structure, a straight line always results on the redox/structure plot (unless, of course, undetected anions or cations are exchanged). Thus, we determine the average density of hexacyanoferrate vacancies from the slope (see eq 3) of the line, and this is what we call the primary structure.

Despite the inability of our analysis method to address issues of compositional and structural heterogeneity in the film, the data clearly show that the primary structure of electrodeposited NiHCF thin films cannot be a "soluble" Prussian Blue analogue, as has been generally assumed. A structure analogous to "insoluble" Prussian Blue can explain many results, both new and old (intercalated waters, nickel/iron ratio, fraction of intercalated cation retained in the oxidized state).

Conclusions

Experimental evidence suggests that the redox active form of electrodeposited NiHCF thin films is more analogous to "insoluble" Prussian Blue, i.e., $A_4Ni_4^{II}[Fe^{II}(CN)_6]_3$, than the "soluble" form, i.e., $A_8Ni_4^{II}[Fe^{II}(CN)_6]_4$. These conclusions are based on correlating EDS measurements of the fractional cation content with Raman measurements of the ferric iron fraction in NiHCF thin films. Our proposed structure is nickel-rich and more open than the previously assumed structure, because of one or more vacant $Fe(CN)_6^{4-/3-}$ sites per unit cell. This revised structure reconciles data in the literature related to H_2O incorporation, and a nickel-rich composition is supported by XPS analysis. Characterization of these deposits by EXAFS is being pursued to better resolve the structure of electrodeposited NiHCF thin films.

Acknowledgment. This work was supported by the DOE Environmental Molecular Science Program (FG07-97ER14819) and the EPA/NSF Technology for a Sustainable Environment Program (CTS-9729046). The authors thank Dr. Deborah Leach-Scampavia for assistance with the collection and interpretation of XPS data. K.M.J. acknowledges the support provided by a NSF Graduate Research Fellowship.

CM010156D

(29) Yamada, S.; Kuwabara, K.; Koumoto, K. *Mater. Sci. Eng. B* **1997**, *49*, 89.